J Mater Sci: Mater Electron (2018) 29:753–761
DOI 10.1007/s10854-017-7969-0

Controllable synthesis of self-assembled MoS_2 hollow spheres for photocatalytic application

Xinchuan Liu[1] · Tinglan Wang[1] · Guangbo Hu[1] · Chao Xu[1] · Yehan Xiong[1] · Yongqian Wang[1,2]

Received: 11 July 2017 / Accepted: 3 October 2017 / Published online: 23 October 2017

Abstract MoS_2 hollow spheres were controllably synthesized with the assistance of surfactant [polyvinyl pyrrolidone (PVP)] through a facile hydrothermal method. Our moderate synthetic route also yielded a large quantity MoS_2 nanospheres and nanosheets by adjusting the additive concentration of PVP. The MoS_2 nanosheets were synthesized without the addition of PVP. With the gradual increase of additive concentration of PVP, the MoS_2 nanosheets assembled into MoS_2 nanospheres and the MoS_2 nanospheres further assembled into the MoS_2 hollow spheres. Meanwhile, a reasonable growth mechanism related to the formation of MoS_2 structures was proposed preliminarily. Moreover, the light absorption and photocatalytic properties of synthesized MoS_2 structures were investigated. The results indicated that MoS_2 hollow spheres exhibited excellent photocatalytic properties, which could be attributed to the unique structure feature, distribution characteristic, abundant of photoactive sites. Thus, it indicated for a huge potential for application in photocatalytic materials, which could solve the water pollution all around the world.

1 Introduction

In recent decades, the environment issue becomes more and more prominent in the world due to improvements in economic growth and our living standards. Among them, the water pollution problem has become increasingly serious [1–4]. Thus, looking for effective methods are urgently required to address global challenges related to this issue. Solar energy is attractive renewable and can be used for photocatalytic degradation of organic pollutants, which is an effective approach used around the world [5]. Therefore, photocatalytic degradation of organic pollutants by utilizing solar energy would possibly offer us clean and sustainable water to meet our demands, which has become one of the most attractive research fields. Plenty of materials have been synthesized and used in the field of photocatalysis [6–12]. In this respect, semiconductor photocatalytic oxidation technology as an effective solution to deal with water purification has received widespread attentions. It has been more and more people's attention due to advantages of low cost, facile synthesis, wide applications [13–15]. To date, most of the photocatalysts are *n*-type metal–oxide semiconductor materials, such as TiO_2 and ZnO. However, the bandgaps of the *n*-type metal–oxide semiconductor materials are too large for most of the visible part of the solar spectrum to be utilized. For example, TiO_2 has a bandgap of 3.2 eV (anatase phase) and just absorbs ultraviolet light which accounted for only 4–6% of sunlight. Thus, TiO_2 usually exhibits a substantially lower photocatalytic activity than expectation and its applications in the field of photocatalysis are limited [16]. It is desirable to look for new semiconductor materials with small bandgaps to harness the solar energy effectively from the visible range and speed up the photocatalytic degradation of organic pollutants.

Molybdenum disulfide (MoS_2), as a typical layered transition-metal dichalcogenide, has drawn increasing attention. S–Mo–S layers in its structure are held together by weak van der Waals force, which has contributed to its unique catalytic, optical and electronic properties [17–20]. Owing

✉ Yongqian Wang
cugwyq@126.com

[1] Faculty of Materials Science and Chemistry, China University of Geosciences, Wuhan 430074, China

[2] Engineering Research Center of Nano-Materials of Ministry of Education, China University of Geosciences, Wuhan 430074, China

to the quantum confinement effects of MoS_2 microsphere, the bandgap of MoS_2 changes from an indirect bandgap of 1.3 eV (bulk) to a direct bandgap of 1.9 eV (few-layers sheets). As a result, it's very effective for visible light absorption. As a transition metal sulfide, MoS_2 can absorb photons to generate electron–hole pairs and then generate high reactivity and strong oxidative hydroxyl radicals which are used for degradation of organic pollutants [21–31]. Furthermore, such a two-dimensional (2D) layered crystal structure provides convenient electron transfer and many active sites for inter facial adsorption. Thus, MoS_2 are suitable for photocatalytic degradation of many compounds including organic pollutants in waste water [32, 33]. As a co-catalyst, the morphology and nanostructure of MoS_2 have considerable effects on the photocatalytic performance. To date, a variety of MoS_2 nanostructures have been fabricated, for example, MoS_2/Bi_2S_3 nanocomposites [34], MoS_2 microspheres [35], MoS_2 nanosheets [36], MoS_2 nanorods and flowerlike MoS_2 [37]. Different techniques like mechanical, chemical vapor deposition and liquid exfoliation have been employed for the synthesis MoS_2 nanostructures. However, the freshly synthesized MoS_2 nanosheets tend to agglomerate together due to their high surface energy and interlayer van der Waals forces, the photocatalytic activity is increased owing to the loss of the edge active sites. To improve the photocatalytic activity, constructing three-dimensional (3D) nanoparticles from two-dimensional (2D) MoS_2 nanosheets is a reasonable approach.

Herein, we report a facile hydrothermal technique to fabricate MoS_2 hollow spheres with the assist of surfactant (PVP). The surfactant plays an important role in the synthesis of products [38]. The structure and morphology of the MoS_2 hollow spheres were fully studied. A reasonable growth mechanism was proposed preliminarily. Moreover, optical and photocatalytic properties of the MoS_2 hollow spheres were also investigated.

2 Experimental details

2.1 Materials and synthesis of MoS_2 hollow spheres

All the chemical reagents were analytical grade and used without purification, in a typical synthesis, 2.0 mmol of ammonium molybdate tetrahydrate [$(NH_4)_6Mo_7O_{24}{\cdot}4H_2O$], 56.0 mmol of thiourea (CH_4N_2S), and 5.0 g PVP were dissolved in 60 mL of deionized water. The mixed solution was stirred for 6 h until the solution was clear and transparent. After that, the solution was transferred into Teflon-lined stainless steel autoclave (80 mL), sealed, and heated in an electric oven at 180 °C for 24 h, followed by natural cooling to room temperature. Subsequently the black products were collected by centrifugation, washed with ethanol and deionized water for several times and then dried at 80 °C for 24 h. Finally, MoS_2 samples was obtained after the products were annealed at 800 °C for 2 h under the protective gas nitrogen condition.

2.2 Characterization

The structure and crystal phase of the as-synthesized MoS_2 samples were characterized by powder X-ray diffraction (XRD, D8 Advanced XRD, Bruker AXS) using a Dmax-3β diffractometer with nickel-filtered Cu K_α radiation. The general morphologies and sizes of the synthesized samples were investigated with field emission scanning electron microscopy (FESEM, SU8010, HITACHI). The FESEM samples were prepared with a thin amorphous gold on their surface. The elemental compositions analysis of the MoS_2 samples was performed by the energy dispersive X-ray spectrometer (EDS) attached to the SU8010 FESEM. The ultraviolet–visible (UV–Vis, UV-2600, Shimadzu) diffuse reflectance spectra was recorded on a GBC spectrometer (Cintra 10 e) equipped with an integrating sphere attachment in the wavelength range of 220–800 nm and a Xe lamp source.

2.3 Photocatalytic tests

Photocatalytic performance of as-synthesized MoS_2 samples were evaluated through measuring the degradation efficiency of methylene blue (MB). Before photocatalytic test, all mixed solution with MoS_2 photocatalysts and MB were placed in dark environment with stirring for 30 min to reach absorption–desorption equilibrium and then the residual concentration of MB was measured. In a typical experiment, a 350 W high-pressure xenon lamp was used as a visible-light source, the lamp was placed 20 cm above the liquid surface. Subsequently, 0.06 g of MoS_2 photocatalysts were added into a 100 mL of 10 mg/L MB aqueous solution. The mixed solution was stirred constantly in the process of experiment. For a given duration (30 min), 4 mL solution was extracted to test the residual concentration of MB, which was evaluated by measuring the change of maximum absorbance in the UV–Vis spectrometry (UV-2600, Shimadzu). The absorption peak at about 664 nm was selected and the residual concentration was obtained through evaluating the intensity ratio between remained and original MB solution. The degradation rate was calculated as following equation:

$$\text{Degradation efficiency}\,(\%) = \frac{C_0 - C}{C_0} \times 100\%$$

where C is the concentration of MB at each irradiated time, and C_0 is the initial concentration when adsorption–desorption equilibrium is achieved.

3 Results and discussions

3.1 Structural and morphological analysis

The phase structure and the elemental compositions of the samples were identified by XRD and EDS respectively. Figure 1a, b shows the typical XRD patterns and the EDS spectrum of the as-synthesized MoS_2 samples obtained by using PVP as additive (83.3 mg/mL). As shown in Fig. 1a, all the diffraction peaks in the patterns can be well indexed to hexagonal MoS_2, which shows good agreement with the standard power diffraction card JCPDS No. 73-1508. For all samples, no additional diffraction peaks related to impurity phase are observed, which indicates MoS_2 nanostructures are obtained. For the MoS_2 samples, the (100), (105) and (110) diffraction peaks become higher and sharper after annealing, and the (103) diffraction peak appears compared to the MoS_2 samples without annealing, indicating crystallinity improvement of MoS_2 crystal. Besides, the diffraction peaks are right shifted, which suggests the decrease of corresponding interplanar spacing caused by the lattice distortion. The diffraction peak corresponding to the (002) plane is from the 2H-MoS_2 structure, thus the (002) reflection is important for investigation of the structure of MoS_2 and describe the layered stacking of the MoS_2 samples. However, it is interesting that the (002) diffraction peak of the MoS_2 samples is very weak after annealing compare with that without annealing, resulting from the strong interaction between MoS_2 and PVP (attached to the surface of MoS_2) through C–S and O–S bonding.

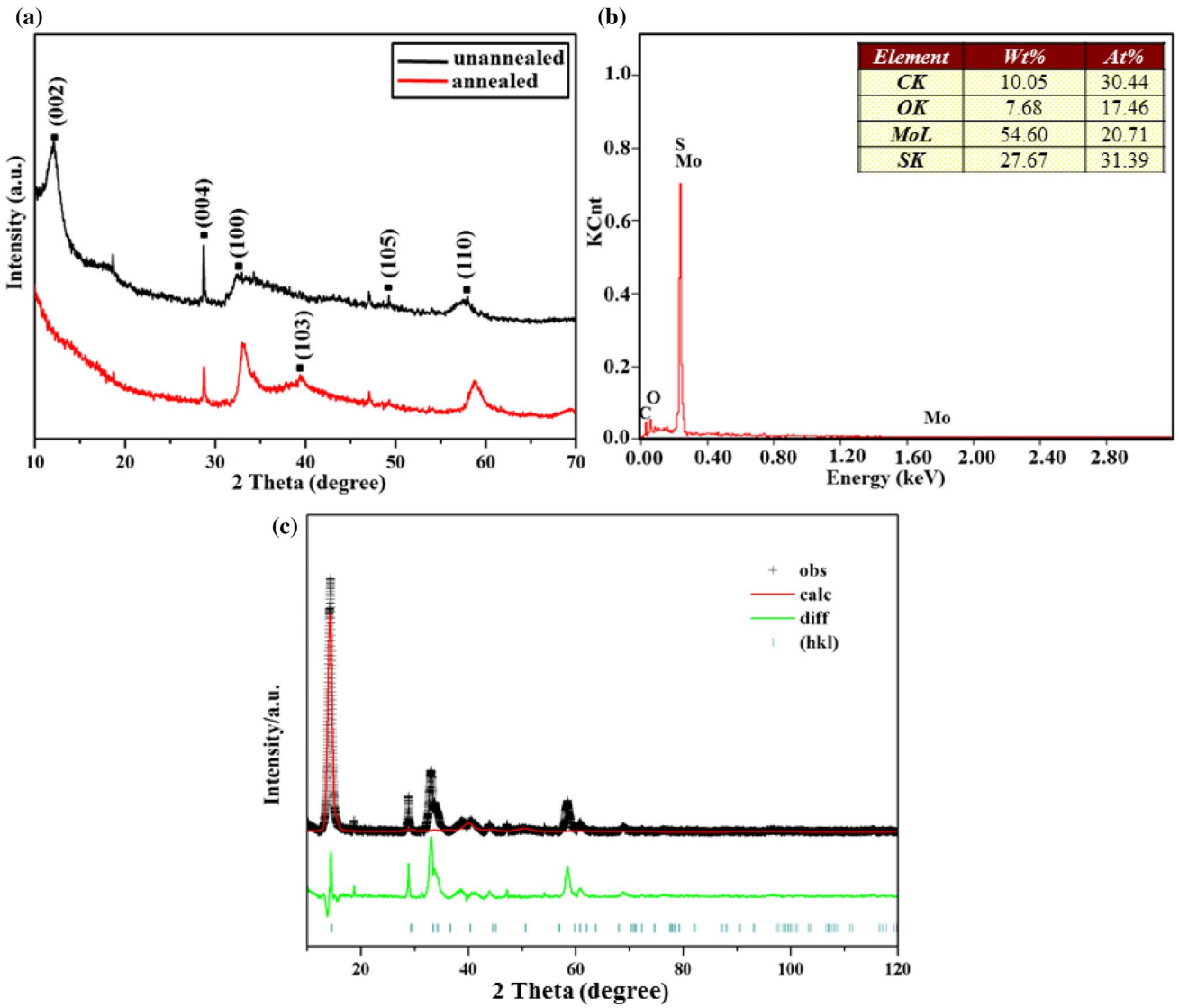

Fig. 1 **a** XRD patterns, **b** EDS spectrum (annealed) of the synthesized MoS_2 samples obtained by using PVP as additive (83.3 mg/mL) and **c** Rietveld refinement pattern of MoS_2 samples obtained without PVP

On this basis, the detailed chemical composition of the MoS_2 samples after annealing is investigated by EDS measurement, as shown in Fig. 1b. The EDS spectrum reveals that the samples are mainly composed of molybdenum element and sulfur element, small amount of carbon element and oxygen element may be mainly derived from the PVP. Figure 1c shows the Rietveld refinement of MoS_2 samples obtained without PVP. According to the refinement data, the obtained MoS_2 crystallizes in a hexagonal phase with space group *P63/mmc* (194), $a=b=3.092$ Å, $c=12.201$ Å, $\alpha=\beta=90°$, $\gamma=120°$, $V=101.053$ Å^3 and $Z=2$. This result verifies that the formation of a single-phase. Based on the above result, it confirms that the MoS_2 is synthesized successfully.

The morphologies of the as-synthesized MoS_2 samples are monitored by FESEM. Figure 2 shows the FESEM images collected from typical areas of the as-synthesized MoS_2 samples. As shown in Fig. 2a, b, we can see that the MoS_2 hollow spheres are synthesized successfully and there are not only complete MoS_2 hollow spheres but also collapsed MoS_2 hollow spheres. Figure 2c-1 shows the FESEM images from a region marked by area 1 (Fig. 2a), as shown in Fig. 2c-1, we can see that the MoS_2 hollow spheres are composed of MoS_2 nanospheres existed one by one independently with diameter of about 200 nm and the MoS_2 nanospheres are distributed uniformly on a large scale. In addition, we can see clearly that each MoS_2 nanosphere is assembled from a lot of rugose-shaped MoS_2 nanosheets, which provides a relatively large surface area for the MoS_2 nanospheres. As a result, photocatalytic performance is significantly improved. Figure 2c-2 shows the MoS_2 nanospheres without annealing. The size of MoS_2 nanospheres is larger and rugose-shaped MoS_2 nanosheets are not obvious, which is compared to that of Fig. 2c-1. It is mainly because annealing can increase crystallinity of MoS_2. What's more, the PVP wrapped on the surface of MoS_2 nanospheres are also removed. The MoS_2 samples to be discussed hereafter are all annealed.

In order to better understand of the formation of the MoS_2 hollow spheres, the experiments of additive PVP with different concentrations are carried out. Figure 3 displays FESEM images of the samples synthesized in different concentration of PVP. It is obvious that PVP plays an important role in the synthesis of MoS_2 hollow spheres. Without the addition of PVP, the synthesized pure MoS_2 samples are composed of MoS_2 nanosheets. However, the MoS_2 nanosheets interact with each other randomly (as shown in Fig. 3a). Besides, the MoS_2 nanosheets agglomerate seriously leading to the relative reduction in surface area, which has an adverse effect on the photocatalytic performance. As shown in Fig. 3b, with the addition of PVP (8.3 mg/mL), the morphologies of the MoS_2 samples change dramatically. The MoS_2 nanosheets interact with PVP and begin to assemble into MoS_2 nanospheres. However, the morphologies of the MoS_2 samples are non-uniform, we can see the unassembled MoS_2 nanosheets and MoS_2 nanospheres assembled by nanosheets. What's more, the assembled MoS_2 nanospheres agglomerate

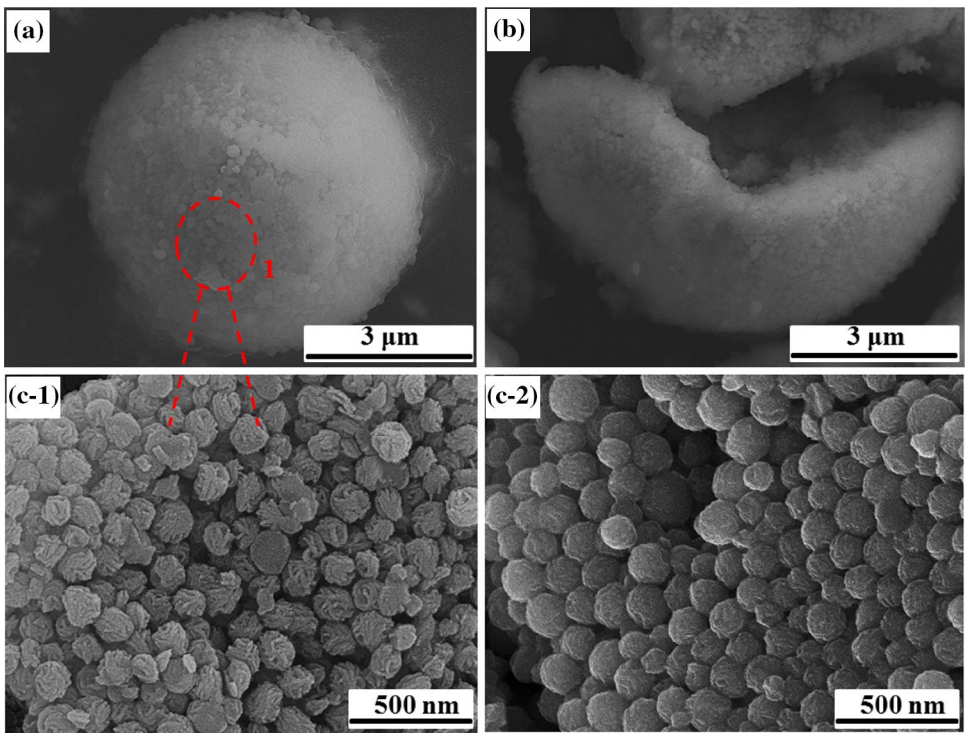

Fig. 2 FESEM images of the MoS_2 samples. **a** MoS_2 hollow spheres (annealed), **b** collapsed MoS_2 hollow spheres (annealed), **c-1** MoS_2 nanospheres from a region marked by area 1 (annealed), **c-2** MoS_2 nanospheres (unannealed)

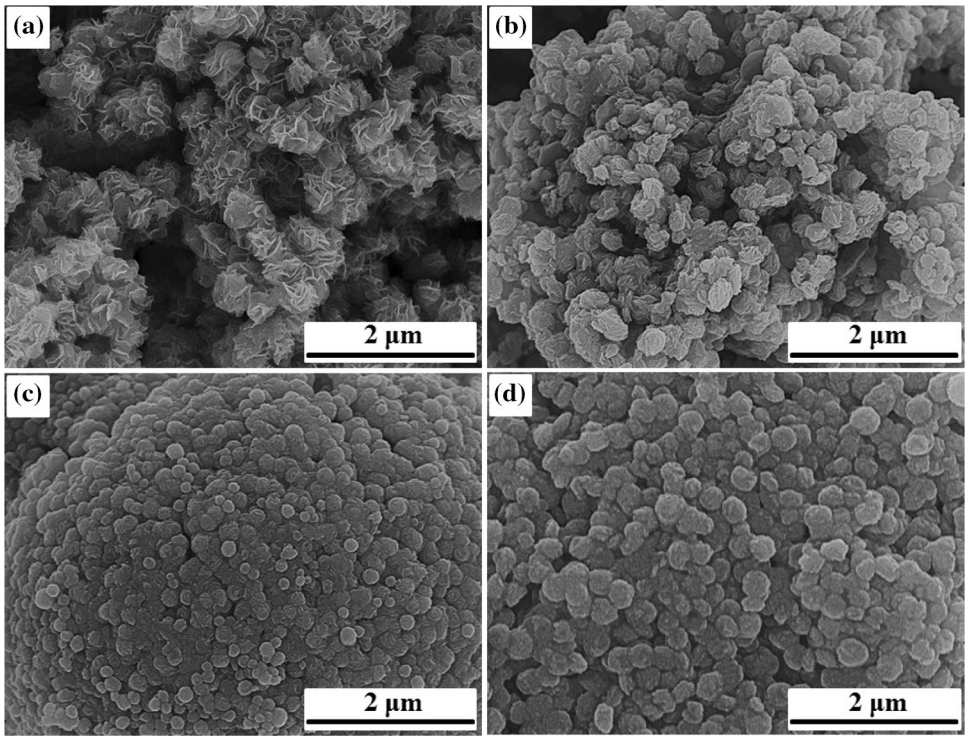

Fig. 3 FESEM images of the MoS_2 samples synthesized in different concentration of PVP, **a** 0.0 mg/mL, **b** 8.3 mg/mL, **c** 16.6 mg/mL and **d** 50 mg/mL

together rather than existence independently. When additive concentration of PVP is 16.6 mg/mL, as shown in Fig. 3c, we can see clearly uniform MoS_2 nanospheres on large scale with diameter of about 100 nm. However, the MoS_2 nanosheets-assembled MoS_2 nanospheres tend to agglomerate together and the size is different. When additive concentration of PVP is 50.0 mg/mL, as shown in Fig. 3d, it is found that uniform MoS_2 nanosheets-assembled MoS_2 nanospheres are synthesized on large scale with diameter of about 150 nm. However, there are still some MoS_2 nanospheres agglomerate together. When additive concentration of PVP is 83.3 mg/mL, as shown in Fig. 2, the as-prepared MoS_2 samples are composed of uniform flowerlike MoS_2 nanospheres which exist independently with diameter of about 200 nm rather than aggregate together. And the MoS_2 nanospheres are synthesized uniformly on a large scale. At the same time, the MoS_2 hollow spheres appeared.

In a word, with the concentration of PVP increasing from 0.0 to 83.3 mg/mL, the morphologies of MoS_2 samples change from nanosheets to nanospheres and the diameter of MoS_2 nanospheres is about 200 nm. What's more, the MoS_2 nanospheres assemble into MoS_2 hollow spheres (additive concentration of PVP is 83.3 mg/mL). The rugose-shaped MoS_2 nanosheets provide a relatively large surface area for the MoS_2 nanospheres and MoS_2 hollow spheres, which is important for photocatalytic behavior.

3.2 Growth mechanism

According to the above experimental results, the formation and growth mechanism of the MoS_2 hollow spheres are preliminarily proposed and are schematically illustrated in Fig. 4.

$$(NH_4)_6Mo_7O_{24} + 3H_2O \rightarrow 7MoO_3 + 6NH_3 \cdot H_2O \quad (1)$$

$$CS(NH_2)_2 + 2H_2O \rightarrow 2NH_3 + H_2S + CO_2 \quad (2)$$

$$4MoO_3 + 2H_2S \rightarrow 4MoO_2 + S + SO_2 + 2H_2O \quad (3)$$

$$MoO_2 + 2H_2S \rightarrow MoS_2 + 2H_2O \quad (4)$$

In the hydrothermal process, the decomposition of ammonium paramolybdate (Eq. 1) and the decomposition of thiourea (Eq. 2) occurred firstly. After that, the MoO_3 derived from reaction (1) react with H_2S derived from reaction (2), as a result, the Mo^{6+} is reduced to Mo^{4+}. At last, the MoO_2 which provides Mo^{4+} react with H_2S which provides S^{2-} to generate MoS_2 nanosheets (Fig. 4a, b). The appearance of a (002) diffraction peak (Fig. 1a) indicates the hierarchical structures of MoS_2 samples. However, the MoS_2 nanosheets interact with each other irregularly and agglomerate together seriously due to the large surface area and high surface activity (Fig. 3a). It is believed that PVP is important for growth of MoS_2 nanospheres and hollow spheres. With addition of PVP (Fig. 4c), the MoS_2 nanosheets spontaneously assemble

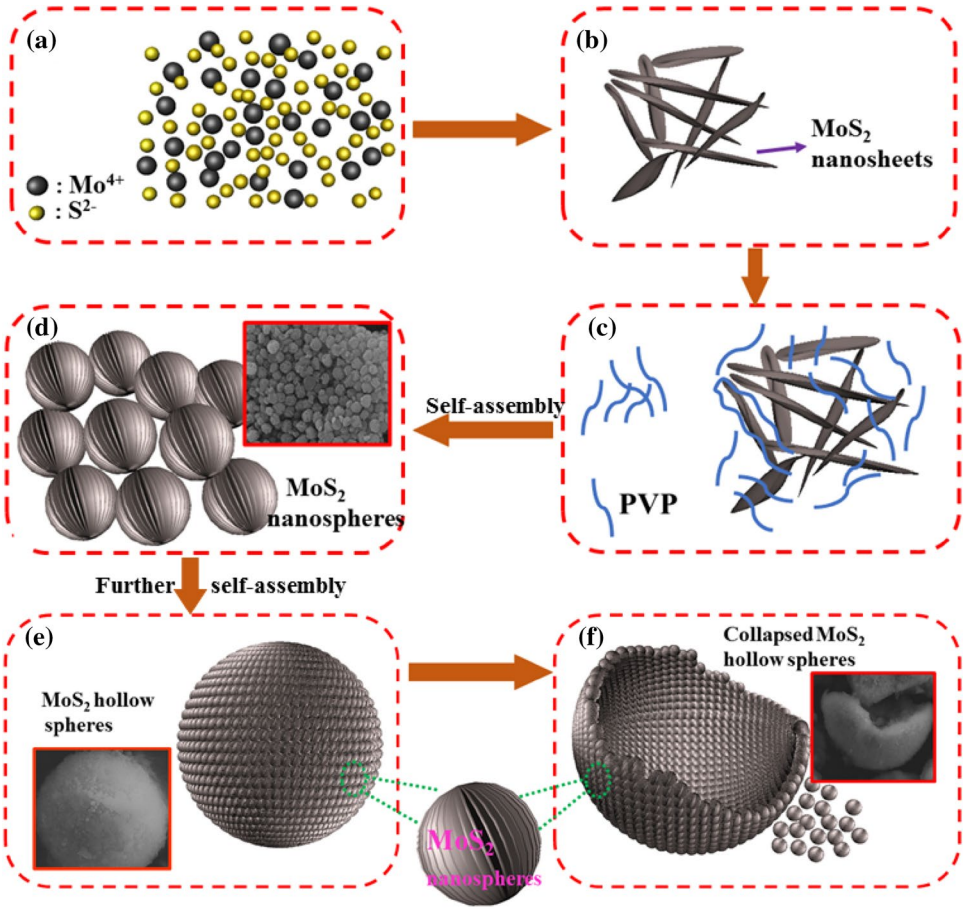

Fig. 4 Schematic illustration for the formation of MoS_2 nanosheets-assembled MoS_2 nanospheres (**a**–**d**) and the MoS_2 hollow spheres (**e, f**)

into MoS_2 nanospheres. Besides, with the concentration of PVP increasing, the size of synthesized MoS_2 nanosheets-assembled MoS_2 nanospheres gradually increases to about 200 nm and the MoS_2 nanospheres changes from agglomerated state to independent state. It is supposed that PVP intertwine to form network structure in solution and adsorb on the surface of MoS_2 nanosheets due to the strong interaction between MoS_2 and PVP. Thus, the MoS_2 nanosheets encapsulated by PVP assemble into MoS_2 nanospheres in high concentration of PVP solution due to winding between PVP (Fig. 4d). Besides, the size of MoS_2 nanospheres assembled by MoS_2 nanosheets is limited to about 200 nm due to the encapsulation of PVP which prevent contact between the MoS_2 particles. Meanwhile, the agglomeration among MoS_2 nanosheets is also limited. However, when the additive concentration of PVP is 83.3 mg/mL, it is found that the MoS_2 nanospheres assembled by MoS_2 nanosheets tend to self-assemble into the MoS_2 hollow spheres (Fig. 4e). MoS_2 nanospheres assembled by MoS_2 nanosheets are also encapsulated by PVP, as mentioned above. PVP molecules in solution tend to form network structure, so the MoS_2 nanospheres self-assemble into MoS_2 hollow spheres owing to the intermolecular forces among PVP molecules. During the synthesis process of the MoS_2 nanospheres self-assembled into MoS_2 hollow spheres, the MoS_2 hollow spheres maintain a good state of spherical structure when the gravity keeps a balance with intermolecular forces and inner stress, if the gravity is greater than the sum of intermolecular forces and internal stresses, the MoS_2 hollow spheres begin to collapse until achieve a new balance (Fig. 6f). Besides, the MoS_2 hollow spheres can provide more surface area for the active sites which are the key factor in the process of photocatalysis.

3.3 Optical properties

The UV–Vis absorption spectra of the MoS_2 hollow spheres and the MoS_2 nanosheets are exhibited in Fig. 5a. We can observe that both the MoS_2 samples have strong light absorption in ultraviolet light and visible light regions. A strong absorption peak can be observed at a short wavelength of 338 nm and a long wavelength of 590 nm for both MoS_2 samples. However, there is a weak absorption peak at wavelength of 654 nm for MoS_2 nanosheets. The MoS_2 hollow spheres show the significant enhancement of photoabsorption intensity in both ultraviolet light and visible light regions compared with the MoS_2 nanosheets, which indicates that the MoS_2 hollow spheres have superior

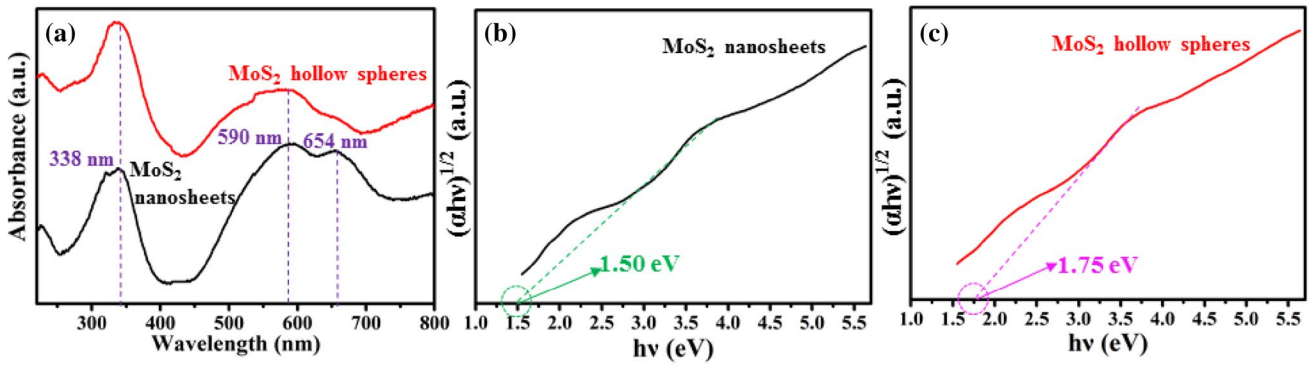

Fig. 5 **a** UV–Vis spectra of MoS_2 nanosheets and MoS_2 hollow spheres, plots of $(\alpha h\nu)^{1/n}$ versus $h\nu$ for **b** MoS_2 nanosheets and **c** MoS_2 hollow spheres

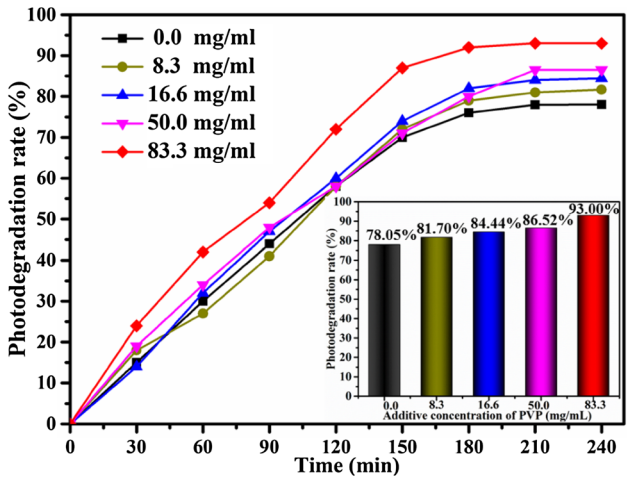

Fig. 6 Photodegradation rate (MB) of MoS_2 samples synthesized in different additive concentration of PVP under visible light. 78.05% (MoS_2 nanosheets), 93.00% (MoS_2 hollow spheres)

photocatalytic performance. The optical band gap energy (E_g) can be calculated from the equation given below:

$$\alpha h\nu = A\left(h\nu - -E_g\right)^n$$

where α is the optical absorption coefficient, h is the Planck constant, ν is the photon frequency, A is the parameter of the electronic structure of the material itself, which is independent of the incident light energy. E_g is optical band gap energy and n is equal to 1/2 and 2 for direct allowed transition (ZnO) and indirect allowed transition (MoS_2). The plots of $(\alpha h\nu)^{1/n}$ versus $h\nu$ for MoS_2 samples are shown in Fig. 5b, c. The value of optical band gap energy (E_g) can be calculated by extrapolating the linear portion of the plot of $(\alpha h\nu)^{1/n}$ versus $h\nu$ to $(\alpha h\nu)^{1/n}=0$. Therefore, the E_g value of MoS_2 nanosheets is evaluated as 1.50 eV as shown in Fig. 5b, the E_g value of the MoS_2 hollow spheres is evaluated as 1.75 eV as shown in Fig. 5c, the E_g of 1.75 eV responds to the wavelength of 697 nm which locates in the visible light region. It indicates that the MoS_2 hollow spheres can absorb visible light.

3.4 Photocatalytic activity

To evaluate the photocatalytic performance of the MoS_2 samples, the photocatalytic experiment is carried out in the presence of MoS_2 samples as catalyst, MB as simulative organic pollutants under the irradiation of a high-pressure xenon lamp (350 W). The results of the photodegradation rate with MoS_2 samples are shown in Fig. 6. As we can see, most of the MB is decomposed after photocatalytic degradation for 180 min with the assistance of MoS_2 samples as photocatalysts. With the increasing of photocatalytic time, the photodegradation rate increases more and more slowly until no longer increasing. The degradation efficiency with the presence of MoS_2 nanosheets reaches 78.05% under the irradiation of visible light for 4 h. With the increasing of additive concentration of PVP, the obtained MoS_2 samples show higher photocatalytic performance under similar situation. The concentration of 8.3, 16.6, 50, 83.3 mg/mL corresponding to the photocatalytic efficiency is 81.70, 84.44, 86.52, and 93.00% (MoS_2 hollow spheres) respectively. The MoS_2 hollow spheres reach the best photocatalytic performance, it may be resulted from the comprehensive effects of strong light absorption and efficient interfacial charge separation. As we all know, owing to the quantum confinement effects of MoS_2 microsphere, the band gap of MoS_2 changes from an indirect bandgap of 1.3 eV (bulk) to a direct bandgap of 1.9 eV (few-layers sheets) which is very effective for visible light absorption. As the synthesized MoS_2 samples, the optical band gap energy change from 1.5 eV (MoS_2 nanosheets) to 1.75 eV (MoS_2 hollow spheres).

As we all know, the structure of MoS_2 is a lamellar structure. According to previous studies, the active site

which determines the photocatalytic performance is present at the edge of the lamellar structure. As for the MoS_2 nanosheets, the lamellar structure itself can provide large numbers of active sites. However, the MoS_2 nanosheets agglomerate together seriously leading to the relative reduction in surface area, which has an adverse effect on the photocatalytic performance. Compared with the MoS_2 nanosheets, the lamellar structure on the surface of the nanospheres can have more active sites related to photocatalytic activity under the same size conditions. What's more, the lamellar structure exists regularly, which can ensure the existence and activity of the active sites. At last, when the MoS_2 nanospheres assembles into MoS_2 hollow spheres, the hollow structure can improve the utilization of nanospheres, which causes better photocatalytic performance than MoS_2 nanospheres. In a word, the lamellar structure on the surface of MoS_2 nanospheres and the unique hollow structure can increase the active surface areas, so abundant of adsorption sites and photoactive sites can be provided. Thus, a mass of high reactivity and strong oxidative hydroxyl radicals used for degradation of organic pollutants can be generated and contribute to the obvious enhancement of photocatalytic properties.

4 Conclusion

In conclusion, MoS_2 hollow spheres are successfully synthesized with a facile hydrothermal method at a soft temperature using PVP as surfactant. By changing the additive concentration of PVP, we achieve a controllable preparation of the morphologies of MoS_2 samples. Without the addition of PVP, the synthesized MoS_2 nanosheets tend to aggregate together due to large active surface areas. With the addition of PVP, the MoS_2 nanosheets begin to assemble into MoS_2 nanospheres with diameter of about 200 nm. The MoS_2 nanospheres assembled by MoS_2 nanosheets tend to assemble into the MoS_2 hollow spheres (the additive concentration of PVP is 83.3 mg/mL). The MoS_2 hollow spheres maintain a good state of spherical structure when the gravity keeps a balance with intermolecular forces and inner stress, if the gravity is greater than the sum of intermolecular forces and internal stresses, the MoS_2 hollow spheres begin to collapse until achieve a new balance. Owing to the unique structure of MoS_2 hollow spheres, the E_g changes to 1.75 eV compared to the MoS_2 nanosheets of 1.5 eV, and the photocatalytic performance is significantly improved. Thus, it is expected to have great application prospect in the field of photocatalysis.

References

1. M.A. Shannon, P.W. Bohn, M. Elimelech, J.G. Georgiadis, B.J. Marinas, A.M. Mayes, Science and technology for water purification in the coming decades. Nature **452**(7185), 301–310 (2008)
2. R.P. Schwarzenbach, B.I. Escher, K. Fenner, T.B. Hofstetter, C.A. Johnson, U.V. Gunten, B. Wehrli, The challenge of micropollutants in aquatic systems. Science **313**(5790), 1072–1077 (2006)
3. C. Liu, X. Xie, W. Zhao, J. Yao, D.S. Kong, A.B. Boehm, Y. Cui, Static electricity powered copper oxide nanowire microbicidal electroporation for water disinfection. Nano Lett. **14**(10), 5603–5608 (2014)
4. B.E. Logan, M. Elimelech, Membrane-based processes for sustainable power generation using water. Nature **488**(7411), 313–319 (2012)
5. K.G. McGuigan, R.M. Conroy, H.J. Mosler, M. du Preez, E. Ubomba-Jaswa, P. Fernandez-Ibanez, Solar water disinfection (SODIS): a review from bench-top to roof-top. J. Hazard. Mater. **235**, 29–46 (2012)
6. A. Ziarati, A. Sobhani-Nasab, M. Rahimi-Nasrabadi, M.R. Ganjali, A. Badiei, Sonication method synergism with rare earth based nanocatalyst: preparation of $NiFe_{2-x}Eu_xO_4$ nanostructures and its catalytic applications for the synthesis of benzimidazoles, benzoxazoles, and benzothiazoles under ultrasonic irradiation. J. Rare. Earth **35**(4), 374–381 (2017)
7. A. Sobhani-Nasab, Z. Zahraei, M. Akbari, M. Maddahfar, S.M. Hosseinpour-Mashkani, Synthesis, characterization, and antibacterial activities of $ZnLaFe_2O_4/NiTiO_3$ Nanocomposite. J. Mol. Struct. **1139**, 430–435 (2017)
8. S.M. Hosseinpour-Mashkani, M. Maddahfar, A. Sobhani-Nasab, Novel silver-doped $NiTiO_3$: auto-combustion synthesis, characterization and photovoltaic measurements. S. Afr. J. Chem. **70**, 44–48 (2017)
9. M. Salavati-Niasari, F. Soofivand, A. Sobhani-Nasab, M. Shakouri-Arani, A.Y. Faal, S. Bagheri, Synthesis, characterization, and morphological control of $ZnTiO_3$ nanoparticles through sol-gel processes and its photocatalyst application. Adv. Powder Technol. **27**, 2066 (2016)
10. A. Sobhani-Nasab, M. Rangraz-Jeddy, A. Avanes, M. Salavati-Niasari, Novel sol-gel method for synthesis of $PbTiO_3$ and its light harvesting applications. J. Mater. Sci. **26**, 9552–9560 (2015)
11. A. Sobhani-Nasab, M. Maddahfar, S.M. Hosseinpour-Mashkani, $Ce(MoO_4)_2$ nanostructures: synthesis, characterization, and its photocatalyst application through the ultrasonic method. J. Mol. Liq. **216**, 1–5 (2016)
12. A. Sobhani-Nasab, M. Sadeghi, Preparation and characterization of calcium tungstate nanoparticles with the aid of amino acids and investigation its photocatalytic application. J. Mater. Sci. **27**(8), 7933–7938 (2016)
13. S. Dong, J. Feng, M. Fan, Y. Pi, L. Hu, X. Han, J. Sun, Recent developments in heterogeneous photocatalytic water treatment using visible light-responsive photocatalysts: a review. RSC Adv. **5**(19), 14610–14630 (2015)
14. M.N. Chong, B. Jin, C.W.K. Chow, C. Saint, Recent developments in photocatalytic water treatment technology: a review. Water Res. **44**(10), 2997–3027 (2010)
15. S. Malato, P. Fernández-Ibáñez, M.I. Maldonado, J. Blanco, W. Gernjak, Decontamination and disinfection of water by solar photocatalysis: recent overview and trends. Catal. Today **147**(1), 1–59 (2009)
16. C. Liu, D. Kong, P.C. Hsu, H. Yuan, H.W. Lee, Y. Liu, P.A. Maraccini, Rapid water disinfection using vertically aligned MoS_2 nanofilms and visible light. Nat. Nanotechnol. **11**, 1098–1104 (2016)

17. S.V. Kershaw, A.S. Susha, A.L. Rogach, Narrow bandgap colloidal metal chalcogenide quantum dots: synthetic methods, heterostructures, assemblies, electronic and infrared optical properties. Chem. Soc. Rev. **42**(7), 3033–3087 (2013)
18. J.H. Rhee, C.C. Chung, E.W.G. Diau, A perspective of mesoscopic solar cells based on metal chalcogenide quantum dots and organometal-halide perovskites, NPG. Asia. Mater. **5**(10), e68 (2013)
19. D. Kong, J.J. Cha, H. Wang, H.R. Lee, Y. Cui, First-row transition metal dichalcogenide catalysts for hydrogen evolution reaction. Energy Environ. Sci. **6**(12), 3553–3558 (2013)
20. X. Gao, H.B. Wu, L. Zheng, Y. Zhong, Y. Hu, X.W.D. Lou, Formation of mesoporous heterostructured $BiVO_4/Bi_2S_3$ hollow discoids with enhanced photoactivity. Angew. Chem. Int. Ed. **53**(23), 5917–5921 (2014)
21. K.S. Novoselov, D. Jiang, F. Schedin, T.J. Booth, V.V. Khotkevich, S.V. Morozov, A.K. Geim, Two-dimensional atomic crystals. Proc. Natl. Acad. Sci. USA **102**(30), 10451–10453 (2015)
22. H. Li, Z. Yin, Q. He, H. Li, X. Huang, G. Lu, H. Zhang, Fabrication of single-and multilayer MoS_2 film-based field-effect transistors for sensing NO at room temperature. Small **8**(1), 63–67 (2012)
23. X. Huang, Z. Zeng, H. Zhang, Metal dichalcogenide nanosheets: preparation, properties and applications. Chem. Soc. Rev. **42**(5), 1934–1946 (2013)
24. J.P. Wilcoxon, T.R. Thurston, J.E. Martin, Applications of metal and semiconductor nanoclusters as thermal and photo-catalysts. Nanostruct. Mater. **12**(5–8), 993–997 (1999)
25. T.R. Thurston, J.P. Wilcoxon, Photooxidation of organic chemicals catalyzed by nanoscale MoS_2. J. Phys. Chem. B **103**(1), 11–17 (1999)
26. Y. Li, Y.L. Li, C.M. Araujo, W. Luo, R. Ahuja, Single-layer MoS_2 as an efficient photocatalyst. Catal. Sci. Technol. **3**(9), 2214–2220 (2013)
27. L. Ge, C. Han, X. Xiao, L. Guo, Synthesis and characterization of composite visible light active photocatalysts MoS_2-g-C_3N_4 with enhanced hydrogen evolution activity. Int. J. Hydrogen Energy **38**(17), 6960–6969 (2013)
28. H.L. Zhuang, R.G. Hennig, Computational search for single-layer transition-metal dichalcogenide photocatalysts. J. Phys. Chem. C **117**(40), 20440–20445 (2013)
29. K. Chang, Z. Mei, T. Wang, Q. Kang, S. Ouyang, J. Ye, MoS_2/graphene cocatalyst for efficient photocatalytic H_2 evolution under visible light irradiation. ACS Nano **8**(7), 7078–7087 (2014)
30. A.K. Singh, K. Mathew, H.L. Zhuang, R.G. Hennig, Computational screening of 2D materials for photocatalysis. J. Phys. Chem. Lett. **6**(6), 1087–1098 (2015)
31. Y. Tan, K. Yu, T. Yang, Q. Zhang, W. Cong, H. Yin, Z. Zhu, The combinations of hollow MoS_2 micro@nano-spheres: one-step synthesis, excellent photocatalytic and humidity sensing properties. J. Mater. Chem. C **2**(27), 5422–5430 (2014)
32. C. Tan, H. Zhang, Two-dimensional transition metal dichalcogenide nanosheet-based composites. Chem. Soc. Rev. **44**(9), 2713–2731 (2015)
33. X. Zhang, Y. Xie, Recent advances in free-standing two-dimensional crystals with atomic thickness: design, assembly and transfer strategies. Chem. Soc. Rev. **42**(21), 8187–8199 (2013)
34. L.L. Long, J.J. Chen, X. Zhang, A.Y. Zhang, Y.X. Huang, Q. Rong, H.Q. Yu, Layer-controlled growth of MoS_2 on self-assembled flower-like Bi_2S_3 for enhanced photocatalysis under visible light irradiation. NPG. Asia. Mater. **8**(4), e263 (2016)
35. S. Ding, D. Zhang, J.S. Chen, X.W.D. Lou, Facile synthesis of hierarchical MoS_2 microspheres composed of few-layered nanosheets and their lithium storage properties. Nanoscale **4**(1), 95–98 (2012)
36. W. Zhou, Z. Yin, Y. Du, X. Huang, Z. Zeng, Z. Fan, H. Zhang, Synthesis of few-layer MoS_2 nanosheet-coated TiO_2 nanobelt heterostructures for enhanced photocatalytic activities. Small **9**(1), 140–147 (2013)
37. L. Ma, L.M. Xu, X.P. Zhou, X.Y. Xu, Biopolymer-assisted hydrothermal synthesis of flower-like MoS_2 microspheres and their supercapacitive properties. Mater. Lett. **132**, 291–294 (2014)
38. M. Ramezani, A. Sobhani-Nasab, S.M. Hosseinpour-Mashkani, Synthesis, characterization, and morphological control of $Na_{1/2}Bi_{1/2}Cu_3Ti_4O_{12}$ through modify sol-gel method. J. Mater. Sci. **26**(7), 4848–4853 (2015)